Renewable Energy 225 (2024) 120234

Contents lists available at ScienceDirect

Renewable Energy

journal homepage: www.elsevier.com/locate/renene

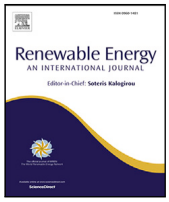

Control co-design and optimization of oscillating-surge wave energy converter

Jeff Grasberger [a], Lisheng Yang [b], Giorgio Bacelli [a], Lei Zuo [b,*]

[a] Sandia National Laboratories, Albuquerque, 87185, NM, USA
[b] Department of Naval Architecture and Marine Engineering, University of Michigan, Ann Arbor, 48109, MI, USA

ARTICLE INFO

Keywords:
Ocean wave energy
Oscillating-surge wave energy converter
Control co-design
Shape optimization
Power-takeoff design

ABSTRACT

Ocean wave energy has the potential to play a crucial role in the shift to renewable energy. In order to improve wave energy conversion performance, it is necessary to break through the traditional sequential design process due to the coupling of subsystems such as the wave capture structure geometry, power take-off (PTO), and control systems. A co-design optimization is introduced in this paper to include effects of all subsystems with one outer and one inner optimization loop in order to reach a fully optimal design of an oscillating surge wave energy converter (OSWEC). A width and height sweep serves as an outer loop geometry optimization while power take-off components and control parameters are optimized efficiently in an inner loop for each geometry. An investigation into electrical power and mechanical power maximization also outlines the contrasting nature of the two objectives to illustrate the importance of electrical power maximization for identifying optimality. The co-design optimization leads to an optimal design with a width of 12 m and a height of 10 m which achieves an improvement in the normalized power value of over 60% when compared to sequential design. A sensitivity analysis of the PTO system enhances understanding of the impact of PTO component value changes to support detailed-design of relevant components including drivetrain and generator. Lastly, the effect of the wave height and period on the optimal design is explored. Through the optimization and sensitivity analysis, a greater understanding on the effects of applying control co-design principles on surface piercing OSWECs is achieved and the importance of control co-design methods is demonstrated.

1. Introduction

As human populations and the dependence on electricity further increase, many of our current energy production methods prove unsustainable. A further reliance on renewable sources of energy is inevitable for our society as extracting oil and gas becomes more expensive due to the dwindling reserves [1], and extraction from renewable sources decreases in price due to improved technology. Due to significant temporal and spatial variation in renewable resources, there will be no one source of renewable energy that can solve all of our energy and climate problems. Each renewable energy resource will play an important role in the transition away from fossil fuels. One of those resources includes the Earth's vast oceans. Specifically, ocean wave power's potential worldwide is estimated at about 2.11 ± .05 TW [2], which is approximately 250 times the annual power production of the U.S. in 2020. Even harvesting a small fraction of this energy could make a big difference in our world's energy issues. A particular benefit of wave energy is the natural seasonal variability that follows the electricity demand in temperate climates [3], making it an ideal clean renewable energy resource to support society's needs.

Harvesting energy from ocean waves has been a lasting challenge for engineers for over half a century. Various methodologies have been applied to the design of wave energy converters (WECs), resulting in a wide variety of devices. Some devices such as heaving point absorbers rely on the rise and fall of surface waves to create energy [4], while other WECs may utilize underwater pressure differences or even air pressure caused by heaving waves [5]. Another type known as oscillating-surge wave energy converters (OSWECs) harvest energy from the surge forces of ocean wave fronts, typically operating in shallow water and rotating around a base which is moored directly to the ocean floor [6]. This type of WEC has gained popularity in the past decade due to its great scalability. Unlike point absorbers whose sizes have to be constrained with respect to the wavelength, OSWECs can be built as large as needed to capture most of the power flux in the waves. This has been demonstrated in several utility scale devices including the Oyster [7] and the WaveRoller [8]. The hydrodynamics properties of OSWEC are investigated by various studies to understand how the surge device's shape influences its power capture capability.

* Corresponding author.
E-mail address: leizuo@umich.edu (L. Zuo).

https://doi.org/10.1016/j.renene.2024.120234
Received 1 June 2023; Received in revised form 20 February 2024; Accepted 27 February 2024
Available online 28 February 2024
0960-1481/

For example, Gomes et al. presented a parametric study of an OSWEC with rectangular flap shapes [9], while Sheng et al. designed and tested a curved shape device and analyzed its power performance [10,11]. With rectangular flaps as the dominant shape investigated so far [12–16], there has been a growing effort to commercialize flap-shaped OSWEC. The US National Renewable Energy Laboratories (NREL) first published the detailed technical and economical data of a reference OSWEC model [17] for this purpose. The focus of the commercialization stage moves beyond power capture capability to the device's cost efficiency, and a proper design should minimize the cost of energy.

Currently, the main design procedure employed in the industry is still a mostly iterative evaluation process [18]. Although there are plenty of design optimization tools developed to speed up the evaluation process [19–23], their adoption rates in the industry are not high. One main reason is that current design optimization tools often fail to comprehensively consider all components of a WEC. With the current tools, the design process often follows a specific, sequential order. First, the geometry of WEC structure, is designed with a certain objective function in mind such as maximizing mechanical power harvested over a cost function such as surface area or volume as in [24,25]. Next, the power take-off (PTO) system is designed to transfer the maximum amount of mechanical energy to harvestable electrical energy as in [26]. Lastly, a control scheme is applied, often with the goal of further maximizing the mechanical power delivered to the device. Potential control methods include passive control, reactive control, phase control, and model predictive control (MPC) [27]. This traditional design process fails to consider the coupling of the WEC system as a whole, and each step in the design process further restricts the future steps. For WECs, the optimal geometric design is affected by both the PTO system employed and the control method, which rely on each other as well. Although a sequential design can lead to optimal controls for the geometry and power take-off considered, the geometry and power take-off may not be optimal for the controls implemented. This concept is explained in a variety of studies, including [28], which suggests the importance of considering accurate electrical power conversion for WEC control design while highlighting the risks associated with a sequential design. A fully optimal design requires synergistic decision making by the engineer to account for the subsystem interactions. Furthermore, realistic considerations such as cost and constraints, which are often overlooked in initial design exploration, can further impact each stage of design. Because of the innate interdepedencies between the WEC subsystems, the sequential design process leads to sub-optimal designs.

A contrasting design philosophy that considers the entire system as well as subsystem interactions is known as co-design [29]. Application of co-design to wave energy converters is limited and previous studies have yet to focus on the design of all subsystems simultaneously. Faedo and Ringwood [30] set up a potential co-design framework, but do not present the results of an application of the framework. O'Sullivan and Lightbody [28] discuss each subsystem and emphasize both mechanical and electrical constraints, but do not consider the effects that the co-design process has on geometric design, thus not fully exploring an important facet of co-design: the restriction that initial geometric design places on subsequent PTO and control design. Recently, Bacelli and Coe [31] suggest a method of consolidating the WEC design into a two-port model and point out the optimal design should try to achieve impedance matching at these two ports. This method is applied and expanded upon later by Ströfer et al. [32] for co-design of a PTO together with controllers. However, they only considered a fixed floater geometry, leaving a significant part of the WEC design out of the loop.

By recognizing the importance of impedance matching across the floater geometry, PTO, and electrical generator current control, this paper formulates a comprehensive optimization problem to maximize the energy transfer from fluid motion all the way to the delivered active electrical power. A holistic perspective to WEC co-design suggested in this paper optimizes the floater geometry, power take-off, and controls simultaneously to maximize the cost-normalized potential electrical power. With the best of the authors' knowledge, this is the first time such a holistic design problem is investigated in the literature. Although the co-design method in this paper is carried out for an oscillating-surge bottom-hinged wave energy converter, it should be versatile enough to be applied to any WEC type.

This paper details the co-design process carried out to optimize the geometry, power take-off, and controls for an oscillating-surge WEC. In Section 2, the hydrodynamics, power take-off dynamics, and controller equations are detailed. The optimization procedure is depicted in Section 3 which shows the setup of the holistic co-design optimization loop. The results of the full geometry optimization considering optimal power take-off and controls are shown in Section 4, which also investigates a comparison to the sequential design process and a sensitivity analysis of the power take-off system. The effects of different sea states are also examined in Section 4. Lastly, Section 5 presents the conclusions of the co-design study performed and suggests future investigations.

2. System modeling

Co-design requires careful consideration of the subsystems involved in design and their interactions. For a wave energy converter, the primary subsystems are the wave capture floater, the power take-off, and the controls. In order to properly assess a design, each of these three subsystems must be taken into account and their dynamics well understood.

2.1. Modeling and simulation of WEC geometry

This co-design study is centered around a bottom-hinged oscillating-surge type WEC, which is essentially a flap pitching about an axis moored directly to the sea bottom. The device itself will be subsequently referred to as a flap. Fig. 1(a) shows the flap's geometry configuration. It has a rectangular shape facing the incoming wave, which makes the flap surge back and forth. Since the flap's bottom is fixed, this surging creates a pitch motion around the y axis which is used to extract power from the wave. The goal of this paper is to optimize the width and height of the flap so that the most power can be obtained for a given capital cost. This is achieved by using the flap's size as a proxy for the device's cost, based on the cost breakdown data provided in [17]. It shows that device structural components, installation, and mooring/foundation costs account for over 75% of the total cost, all of which directly correlates to the flap size. The baseline geometry parameters used in this study are shown in Fig. 1(b). From this side-view it can be seen the flap has a 1.7 m high opening at the bottom and pierces above the free water surface by 1 m. The bottom opening helps reduce material while having little impact on the flap's hydrodynamics properties. The surface piercing configuration helps increase the wave force [9]. This configuration is kept the same for all the (width, height) pairs considered later, meaning all the different flap shapes pierce 1 m above the water and have two legs with the same cross section 1.7 m $\times$ 0.5 m.

In this paper, the flap's hydrodynamics properties are described using linear potential flow theory. A radiation problem for hydrodynamic responses and a diffraction problem for wave excitation are solved using an open-source boundary element method (BEM) software Capytaine [33,34]. BEM solvers numerically integrate water pressure on the flap's surface for waves of different frequencies. A mesh for the surface thus needs to be generated and Gmsh [35] is used for meshing the geometry. Fig. 2 shows the meshing result of the baseline flap.

The flap hydrodynamics can be modeled with a focus on the mechanical impedance of the structure. The mechanical impedance is defined as the input torque divided by the output rotational velocity. First, the input torque can be related to the flap's motion in the time

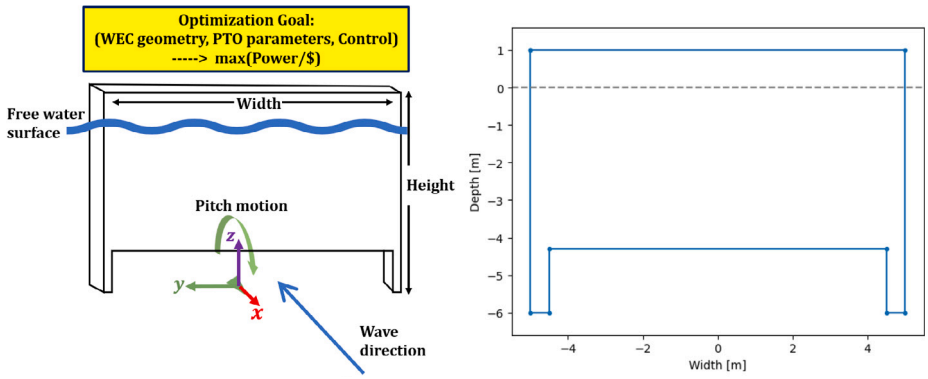

(a) Flap shape to be optimized (b) Baseline geometry

Fig. 1. OSWEC flap model geometry and optimization goal.

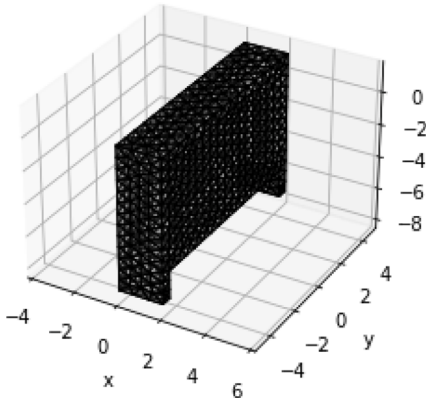

Fig. 2. Flap mesh.

domain in Eq. (1) and frequency domain in Eq. (2). These definitions apply to the pitch motion of the device.

$$\tau(t) = (I + I_A(\infty))\ddot{\theta}(t) + \int_0^t h_r(t-s)\dot{\theta}(s)\,ds + C_{hs}\theta(t) \tag{1}$$

$$T(\omega) = -\omega^2(I + I_A(\omega))\Theta + R(\omega)j\omega\Theta + C_{hs}\Theta \tag{2}$$

In the above equations for torque, θ is the rotational position, ω is the wave frequency in rad/s, I and $I_A(\omega)$ correspond to the inertia and added inertia (at different frequencies) in the pitch direction, respectively, h_r is the radiation convolution kernel as defined in the Cummins equation, $R(\omega)$ is the radiation damping at different frequencies, and C_{hs} is the linear hydrostatic restoring coefficient. The added inertia, radiation damping, and restoring coefficient are each calculated using BEM and are functions of the wave frequency.

By dividing the torque by the velocity ($j\omega\Theta$), the flap's mechanical impedance Z_i can be defined as (Eq. (3)).

$$Z_i(\omega) = j\omega(I + I_A(\omega)) + R(\omega) + \frac{C_{hs}}{j\omega} \tag{3}$$

The mechanical impedance presents a transfer function by which the excitation forces caused by the waves can be easily related to the response of the WEC in terms of rotational velocity.

The impedance can be used to understand the WEC dynamics further through the natural or resonance frequency [36]. The natural frequency can be defined as the point at which the imaginary portion of the complex mechanical impedance is equal to zero. A bode plot of the impedance can be created to identify the natural frequency. The impedance for the baseline flap geometry is displayed in Fig. 3. The natural frequency for this design is shown on the plot as the frequency at which the phase crosses 0 degrees.

The natural frequency is an important part of any WEC design and can help identify effective designs, but it is important to understand that it is not always as simple as designing the natural frequency to match wave frequency. The concept of co-design requires recognition that the power take-off and control dynamics also affect the dynamics of the entire system. Furthermore, small natural frequencies (large natural period) and tight motion constraints that are characteristic to oscillating-surge WEC's [6] mean that designing an OSWEC to match the natural frequency of waves will both be difficult and likely ineffective. When a device oscillates at its natural frequency, the motion is enhanced, the benefits of which would be eliminated with tight motion constraints.

With an understanding of the torque input and the flap's impedance relationship, the maximum potential power, also known as the upper bound for energy harvested from a wave energy converter, can be calculated [37]. For the bottom-hinged flap, this value is defined by Eq. (4) based on the wave pitch excitation torque (T_{exc}) around the bottom hinge and flap impedance and provides a reference for comparison to the actual harvesting potential.

$$P_{UB} = \frac{|T_{exc}|^2}{8Real(Z_i)} \tag{4}$$

2.2. PTO modeling

The power take-off system for this wave energy converter design is a rotary mechanical PTO consisting of a drivetrain and a generator as illustrated in Fig. 4. This PTO design was chosen due to its simplicity and applicability as shown in [26]. The simple PTO model supports efficient optimization at this early stage of design, yet effectively takes into account the desired dynamics such as the mechanical and electrical damping.

As the device rotates about its hinge, a belt system attached to the top of the flap drives the PTO system.

The PTO design can be broken down into the following parameters and components.

- N - gear ratio
- K_t - torque constant
- Z_d - drivetrain impedance
- Z_m - motor impedance
- Z_c - controller impedance
- Z_L - load impedance

The gear ratio represents the motion amplification of the belt transmission system which transfers the rotation of the flap to the rotation of the drivetrain shaft (Eq. (5)).

$$\dot{\theta}_{shaft} = \dot{\theta}_{flap}N \tag{5}$$

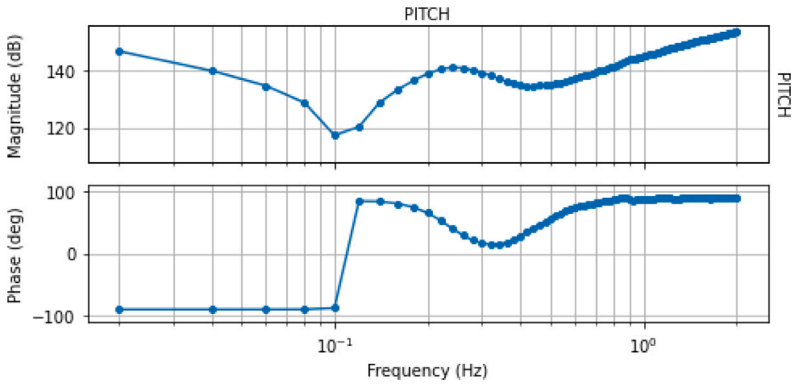

Fig. 3. Mechanical impedance of the baseline OSWEC flap.

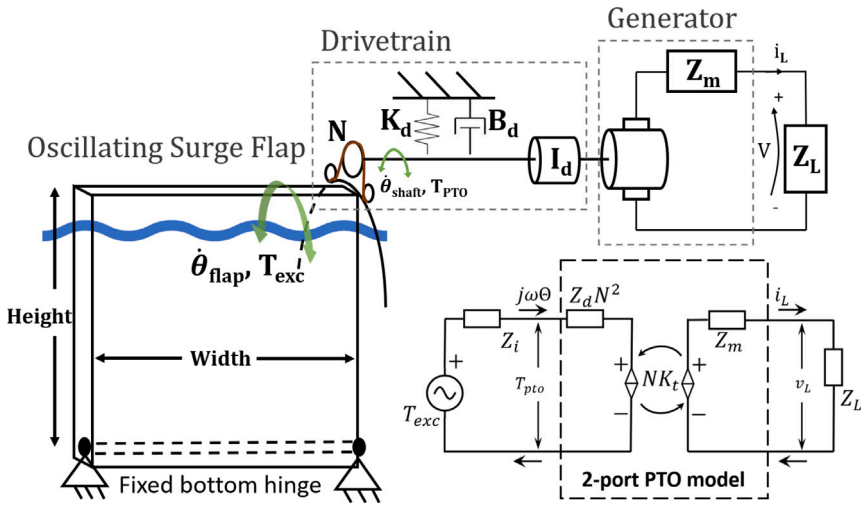

Fig. 4. Diagram of the power take-off design for the oscillating-surge WEC.

The drivetrain is then used to transfer energy along the shaft to the generator. Drivetrain impedance consists of the drivetrain's inertia (I_d), damping (B_d), and stiffness (K_d).

$$Z_d = j\omega I_d + B_d + \frac{K_d}{j\omega} \tag{6}$$

The generator impedance Z_m is defined as the voltage on the generator leads divided by the current. It depends on its winding resistance (R_w) and inductance (L_w).

$$Z_m = j\omega L_w + R_w \tag{7}$$

Note that a DC motor model is adopted here since commonly used three phase AC motors can be equivalent to a DC motor after a rotary frame transformation. With the drivetrain and generator impedance defined, the PTO is modeled as a two-port network as shown in Fig. 4. The input to the left side of the 2-port network corresponds to the PTO torque T_{PTO} as the effort variable, and the resulting flow variable is the flap's rotational velocity $j\omega\Theta$. The output on the right side of the 2-port network corresponds to the load current i_L as the resulting flow variable, and the effort variable is the voltage across the load (v_L), while Z_L represents the load impedance.

In accordance with the two-port model, the effort variables (torque and voltage) can be formulated in terms of the flow variables (Eqs. (8) and (9)). Then, the PTO impedance matrix can be constructed in Eq. (10) with $V_{pitch} = j\omega\Theta$ representing the pitch rotational velocity of the flap. Note that all the equations are written in frequency domain and thus (ω) is dropped from the variables for simplicity.

$$T_{PTO} = N^2 Z_d V_{pitch} - K_t N i_L \tag{8}$$

$$v_L = K_t N V_{pitch} + Z_m i_L \tag{9}$$

$$\begin{bmatrix} T_{PTO} \\ v_L \end{bmatrix} = [Z_{PTO}] \begin{bmatrix} V_{pitch} \\ i_L \end{bmatrix} = \begin{bmatrix} Z_{11} & Z_{12} \\ Z_{21} & Z_{22} \end{bmatrix} \begin{bmatrix} V_{pitch} \\ i_L \end{bmatrix} = \begin{bmatrix} N^2 Z_d & -K_t N \\ K_t N & Z_m \end{bmatrix} \begin{bmatrix} V_{pitch} \\ i_L \end{bmatrix} \tag{10}$$

The average electrical power harvested by the load can now be defined by Eq. (11). The coefficient $\frac{1}{2}$ corresponds to the root-mean-square (rms) value for current.

$$P_L = \frac{1}{2}|i_L|^2 R_L \tag{11}$$

The load resistance (R_L) is simply understood as the real part of the load impedance. The current, on the other hand, requires a more complex derivation. Ultimately, it is desired to derive the load current in terms of the wave excitation torque (T_{exc}). The transfer function from velocity to current can be derived from the 2-port model (Eq. (12)) and the excitation torque can be related to the velocity in Eq. (13) with Z_{in} as the input impedance based on the voltage gain from the 2-port model.

$$\left|\frac{i_L}{V_{pitch}}\right| = \left|\frac{Z_{21}}{Z_L + Z_{22}}\right| \tag{12}$$

$$T_{exc} = V_{pitch}(Z_i + Z_{in}) = V_{pitch}\left(Z_i + Z_{11} - \frac{Z_{12}Z_{21}}{Z_L + Z_{22}}\right) \tag{13}$$

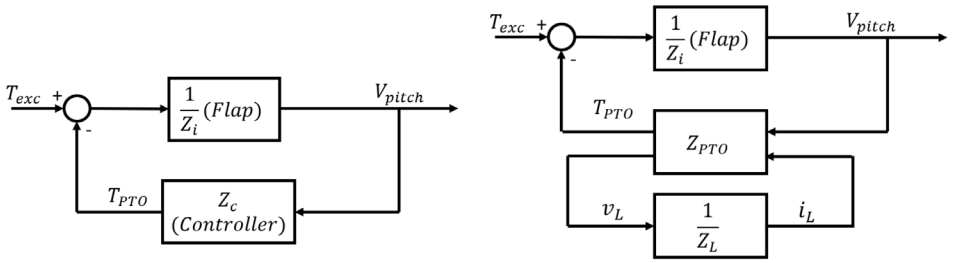

(a) Assumed controller (b) Corresponding load

Fig. 5. Design load impedance for a controller.

By solving for the velocity V_{pitch} in Eq. (13) and plugging into Eq. (12), i_L can be written in terms of T_{exc} (Eq. (14)).

$$i_L = \left|\frac{Z_{21}T_{exc}}{(Z_{11}+Z_i)(Z_{22}+Z_L)-Z_{12}Z_{21}}\right| \tag{14}$$

Substituting the PTO impedance elements into Eq. (14) and solving for the average electrical power from Eq. (11) yields Eq. (15) for the average electrical power delivered to the load in the frequency domain.

$$P_L = \frac{-K_t^2 N^2 |T_{exc}|^2 Real(Z_l)}{2\left|(N^2 Z_d + Z_i)(Z_m + Z_L) + K_t^2 N^2\right|^2} \tag{15}$$

The above equation provides a quick but effective way to take into account the power take-off components in the calculation of electrical power and will be used for PTO parameter optimization in this study.

2.3. Controller modeling

WEC controllers are used to regulate the force/torque applied by the PTO on the oscillating system. The objective of control is to adjust the WEC's motion according to the incoming waves so that the most mechanical energy can be captured from the waves to the wave capture structure (the flap in this paper). However, control force/torque needs to be exerted through the PTO mechanism onto the flap, and losses will be incurred in this process diminishing the eventual electrical energy delivered to the load. Therefore, a control co-design process is needed to design the optimal PTO for a certain flap geometry so that the PTO can track desired control commands in a broad range to increase mechanical power capture while not incurring excessive losses that may offset the increased power capture. To perform such kinds of co-design, ideally taking the controller that will be actually implemented can provide the most accurate optimization results. But in the design phase the ultimate control to be used is often undecided, and it is also too computationally prohibitive to run a time domain controller such as MPC inside a design optimization loop. Therefore, a simpler controller structure, which can be indicative of a real controller's performance through the optimized PTO is more suitable for the optimization routine. In this paper, a PI controller is used for this purpose as suggested by [38]. The PI controller has advantages in that it only introduces two more parameters. As shown in Eq. (16), the impedance for a PI controller is a function of the proportional (K_p) and integral (K_i) gains being applied.

$$Z_c = K_p + \frac{K_i}{j\omega} \tag{16}$$

For the design optimization the controller can be assumed to directly command the PTO torque applied on the flap based on the flap's rotational velocity as shown in Fig. 5(a). In reality this control needs to be fulfilled by the PTO through controlling the load current and voltage. Therefore, an equivalent load impedance needs to be derived so that the PTO can execute the dictated control law (Fig. 5). In order to relate the load impedance to its corresponding controller, the 2-port power take-off model Eq. (10) is used to derive the relationship between i_L, v_L and T_{PTO}, V_{pitch}.

Then an Eq. (17) can be established based on the equivalence between Figs. 5(a) and 5(b). After using Eq. (12) to substitute V_{pitch} by i_L and rearranging the equation, the load impedance is expressed as a function of the controller impedance as shown in Eq. (18).

$$Z_c = \frac{T_{PTO}}{V_{pitch}} = \frac{N^2 Z_d V_{pitch} - K_t N i_L}{V_{pitch}} \tag{17}$$

$$Z_L = \frac{K_t^2 N^2}{Z_d N^2 - Z_c} - Z_m \tag{18}$$

3. Optimization formulation and setup

A proposed co-design optimization procedure is displayed in Fig. 6. In the outer loop, the geometry is defined and the hydrodynamic parameters calculated using Capytaine (Section 3.1). Within the inner optimization loop, the power take-off parameters are first optimized (Section 3.2) together with a simple PI controller which gives an analytical formulation of the average power. Then an unstructured controller is numerically optimized using pseudospectral methods to maximize the electrical power while considering amplitude constraints (Section 3.3). By looping through a series of geometries (candidates) and determining optimal controls and power take-off parameters for each, a brute force outer optimization loop is achieved for which a design objective can be evaluated to determine an optimal design from the candidate designs.

3.1. Geometry optimization procedure

For the geometry analysis portion of this paper, a simple parameter sweep of the width and height of the flap is performed while optimizing the PTO and controls for each geometry and examining the results. The width and height here refer to the cuboid part of the flap and does not include the two legs at the bottom. A range of 2–20 m was considered for height and 4–40 m was considered for the width of the flap (Fig. 7), leading to 100 different shapes of various width to height ratios to consider. Because the WEC is bottom hinged, the water depth is also increased with increasing WEC height, changing the available wave power. The thickness was set as 2 m for most of the shapes except those shapes of smaller sizes. Specifically, in order to maintain a flap-like shape, the thickness of the flaps with long edge smaller than or equal to 8 m is reduced to 1/5 of the long edge length. For flaps of larger sizes, thickness is kept constant since it has little effect on the flap's hydrodynamic properties [9].

For any design analysis, the objective function is paramount. Although extracted power is very important for WEC design, cost is also a significant factor. A balance needs to be found to minimize cost while maximizing usable power. At the early design stage a simple cost proxy based on design parameters helps reduce computation complexity and also provides reasonable estimation. It is noted in [39] that the surface

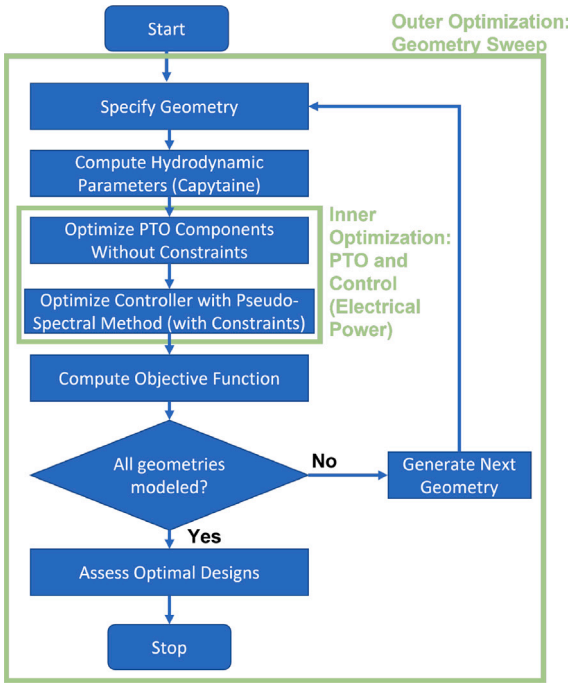

Fig. 6. Co-design optimization loop for oscillating-surge WEC.

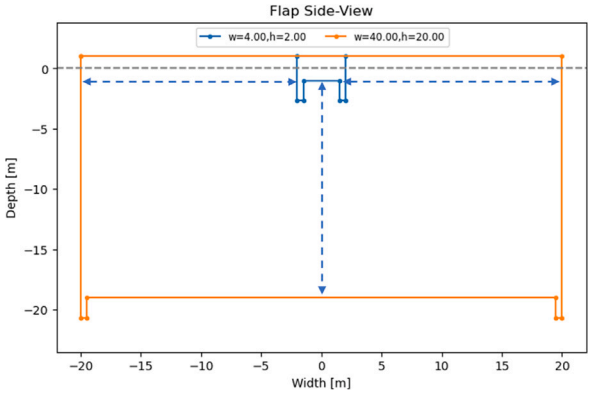

Fig. 7. Diagram showing side-view of the flap's width and height range considered for geometry optimization.

area for full-scale WECs is a good proxy for their costs. In addition, the cost breakdown in [17] shows that the total cost of an OSWEC can be divided into two parts. One part includes structural components, foundation, and installation, and they are largely proportional to the WEC's size. Another part includes PTO, infrastructure, and miscellaneous expenses and does not increase with sizes as much as the first part. Therefore, a two part cost proxy is adopted based on the flap's surface area, which is defined as the surface area of the cuboid part without including the two legs. The first part cost increases linearly with the flap's surface area. The second part cost is assumed to increase logarithmically with surface area. Suppose the two part costs of the smallest flap is known as the base costs C^1_{base} and C^2_{base}, other flaps' costs can be calculated as (Eq. (19)) where A_{surf} represents the surface area. Furthermore, C^1_{base} and C^2_{base} can be expressed as $k_1 A_{base}$ and $k_2 A_{base}$ with $k_1 : k_2$ reflecting the ratio between the two kinds of costs for the smallest flap. Then the objective function considered for analysis in this paper is the cost normalized electrical power shown in (Eq. (20)). Note that since the common factor does not matter in the objective optimization, k_1 and k_2 can be chosen arbitrarily as long as their ratio is correct.

$$Cost = C^1_{base}(A_{surf}/A_{base}) + C^2_{base}(1 + log_n(A_{surf}/A_{base})) \tag{19}$$

$$\max F = \frac{\overline{P_{elec}}}{k_1 A_{surf} + k_2 A_{base}(1 + log_n(A_{surf}/A_{base}))} \tag{20}$$

Through examination of the above objective function, an optimal geometry which takes into account optimal PTO and controls can be selected.

3.2. Power take-off co-optimization procedure

According to the mechanical power take-off model detailed in Section 2.2, the electrical power can be formulated based on the excitation torque, the flap impedance, and the previously defined PTO parameters and impedances. Hence, the PTO optimization problem (assuming PI control) can be expressed by Eq. (21).

$$\min f = \frac{-K_t^2 N^2 |T_{exc}|^2 Real(Z_L)}{2|(N^2 Z_d + Z_i)(Z_m + Z_L) + K_t^2 N^2|^2}$$

subject to:

$$250 \le N \le 500$$

$$.1 \le K_t \le 12 \text{ N m/A}$$

$$2 \le I_d \le 20 \text{ kg m}^2$$

$$-1e9 \le K_p \le 1e9 \text{ N m s/rad}$$

$$-1e9 \le K_i \le 1e9 \text{ N m/rad} \tag{21}$$

The design variables for this optimization are the gear ratio (N), torque constant (K_t), drivetrain inertia (I_d), proportional gain (K_p), and integral gain (K_i), which are each subject to constraints according to what was determined to be reasonable design limits. For instance, the drivetrain shaft itself is expected to have an innate inertia value of about 2 kg m^2, meaning it would be unreasonable to expect a lower value for drivetrain inertia without compromising the strength of the system. On the other hand, a drivetrain inertia over 20 kg m^2 may require a larger flywheel than is physically possible within the drivetrain dimensions. Although the constraints listed are not strictly measured values, they provide a range of feasible designs to be assessed by the optimization algorithm. The initial values used for the PTO component optimization were determined based on the baseline design before optimization. Baseline:

- N = 350
- K_t = 3 N m/A
- I_d = 6 kg m^2

The other variables from Eq. (15) are the excitation torque (determined by wave conditions), flap mechanical impedance, and other components listed below (based on a similar WEC device in [26]), which were kept constant to simplify the optimization problem. Constants:

- R_w = .038 Ω
- L_w = 1.4 mH
- B_d = 2 N m s/rad
- K_d = 0 N m/rad

Note that both generator winding resistance and drivetrain damping only dissipate energy which can otherwise be harvested. Therefore any optimization of them will lead to the lowest boundaries, so they are left out of the optimization. The winding inductance and drivetrain stiffness are kept constant in this study mainly due to practical reasons. However, it is encouraged to explore their effects further in future studies. The optimization problem is solved for multiple cases throughout this paper using SciPy's [40] minimization function with a tolerance of $1 * 10^{-6}$. At this stage the controller structure is simplified to allow for an analytical expression of the objective power function to be optimized in the frequency domain for a specific wave spectrum.

This simplification is based on the observation that a PI controller can approximate the theoretical power upper bounds very well [38]. Although it is convenient to perform the PTO co-optimization entirely in the frequency domain, the drawback is that the optimization cannot enforce time domain operation constraints. Therefore, it is necessary to further optimize the power in the time-domain with constraints enforced. For ease of computation, PTO parameters are kept the same in this last step of optimization and an unstructured controller is adopted to find the upper bound power in the time domain. As mentioned in [31], the optimal PTO should always maximize the power transfer from the wave capture floater to the load. Therefore, operation constraints are deemed as having little influence on the optimal PTO, making it possible to compute the final optimal control separately.

3.3. Control optimization procedure

Since the electrical power evaluated in the frequency domain does not factor in constraints, which are especially important for an OSWEC due to its limited rotation angle, explicit solutions of time-domain optimal control trajectories are needed to obtain the achievable power under practical constraints for each design. The process utilized for time-domain control optimization in this study is known as the pseudo-spectral method [41]. The pseudo-spectral method aims to solve the optimal control problem (22) by parameterizing each variable's time trajectory using a set of harmonic base functions. As such the control trajectory can have as many degrees of freedom as the number of harmonic base functions, allowing an upper bound achievable power to be obtained by not restricting the controller structure.

$$\begin{aligned}
&\min \overline{P_{elec}(t)} = \overline{v_L(t) i_L(t)} \\
&\text{subject to:} \\
&I\ddot{\theta}_{flap} = \tau_{exc}(t) + \tau_{rad}(t) + \boldsymbol{\tau_{PTO}(t)} + \tau_{hs}(t) \\
&|\theta_{flap}| \leq \theta_{max} \\
&|\tau_{PTO}| \leq \tau_{max}
\end{aligned} \tag{22}$$

In the above optimization setup, τ_{rad} is the radiation torque including added inertia and radiation damping terms in Eq. (1), τ_{hs} is the torque due to buoyancy, and θ_{flap} is the WEC rotational position. τ_{PTO} is the control variable to be optimized. Each of these terms is parameterized by a set of harmonic bases, and the optimal control problem is then transcribed into a nonlinear programming program where the dynamics is transcribed to equality constraints. Since the load voltage and current $v_L(t)$ and $i_L(t)$ are not included in the dynamics, a method that can convert the controlled PTO torque and resulting flap velocity directly to the load current and voltage is desirable in order to assess the electrical power provided by the controller. The PTO impedance matrix (Eq. (10)) is then rearranged into its ABCD form [42] in Eq. (23). Although this linear transformation is derived in the frequency domain, it can readily be used for the pseudo-spectral method as all the time domain trajectories are already transcribed to a sum of harmonic functions.

$$\begin{bmatrix} i_L \\ v_L \end{bmatrix} = [Z_{ABCD}] \begin{bmatrix} V_{pitch} \\ T_{PTO} \end{bmatrix} = \begin{bmatrix} -Z_{12}^{-1} Z_{11} & -Z_{12}^{-1} \\ (Z_{21} - Z_{22} Z_{12}^{-1} Z_{11}) & Z_{22} Z_{12}^{-1} \end{bmatrix} \begin{bmatrix} V_{pitch} \\ T_{PTO} \end{bmatrix} \tag{23}$$

The pseudo-spectral method is advantageous for early-stage design optimization for two reasons: the ability to take into account constraints and the use of the unstructured controller. It would be much more computationally expensive to simulate an entire model predictive controller (MPC) for each potential design, so taking into account constraints within optimization allows for quick, yet effective controls. Despite not using a computationally expensive controller, the pseudo-spectral method still provides a fair estimation of the upper bound power a real-time controller can achieve. This is because in this method the wave excitation is converted from the known frequency domain. Therefore, the wave excitation is known precisely for the optimized timeframe. In addition, the WEC's dynamics is assumed to be known precisely for the controller for the whole timeframe. In comparison, a real-time controller would often need to have a wave forecaster to predict the future wave excitation, and an estimator to estimate the dynamics, both of which introduce additional errors resulting in less power. Moreover, to allow real-time operation the control degree of freedom may be limited leading to suboptimal results as compared to the full degree of freedom unstructured controller. Although this pseudospectral method may overestimate power, it serves the purpose of aiding design decisions as it inflates power universally for all designs but preserves the trend.

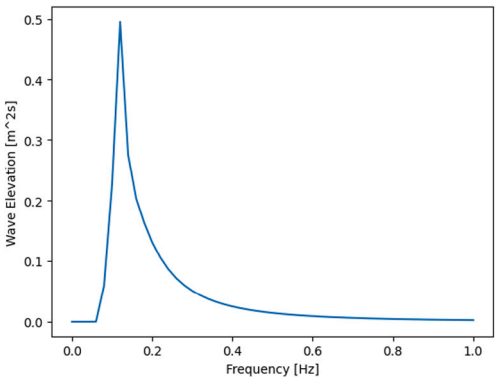

Fig. 8. Wave elevation spectrum vs. frequency for JONSWAP wave with height of 2 m and period of 8.33 s.

With the advantages discussed above, an unstructured controller provides an appropriate method to quickly assess optimal controls that take constraints into account. During each iteration of the optimization, the frequency domain PTO torque (controlled variable) and WEC response are established at each frequency defined by the BEM data. A fast Fourier transform converts the results to the time domain to allow the constraints to be evaluated. Based on the results of the iteration in terms of objective function (average electrical power) and constraint satisfaction (or lack thereof), the controlled PTO torque over the timeframe is changed for the next iteration. This process is repeated until the optimization algorithm (SLSQP) converges on a set of PTO torques which maximize average harvested electrical power while satisfying constraints. Essentially, the frequency domain calculation allows the entire simulation timeframe to be solved simultaneously, meaning the average power over the simulation can be easily assessed for each optimization iteration. Thus, the unstructured controller, which can apply a unique and optimized PTO force at each timestep, is aptly used for the co-design optimization procedure in this study.

4. Simulation results and discussion

4.1. Optimization results

After characterizing the WEC model and the optimization procedure, the expected wave conditions can be defined. Ocean waves are often characterized in terms of regular waves or irregular waves. Regular waves consist of one single frequency and wave height. Irregular waves, on the other hand, include a combination of frequencies with different heights and frequencies and are often defined by a spectrum such as the JONSWAP spectrum [43]. In this study, an irregular JONSWAP wave ($\gamma = 3.3$) with a significant height of 2 m and a characteristic period of 8.33 s is considered. The spectrum is shown in Fig. 8 and a 50 s wave elevation example from the spectrum is shown in Fig. 9.

In order to determine an optimal geometric design, the height and the width of the flap were varied according to Fig. 7. As shallow water,

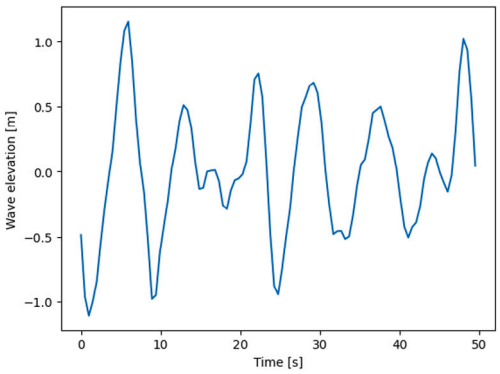

Fig. 9. Wave elevation time-series for JONSWAP wave with height of 2 m and period of 8.33 s.

bottom mounted OSWECs are considered here, the water depth used in the hydrodynamics computation changes when the flap height changes (The water depth was set to 2 m plus the flap height). This leads to different wave power potential for different designs. Moreover, as the same wave spectrum is considered across different shapes, for flaps with lower heights, the water is shallower and the wave's nonlinearity becomes stronger. This to a degree contradicts the linear wave assumption adopted for the hydrodynamics computation based on the potential flow theory. Nevertheless, the inaccuracy is deemed acceptable especially considering the shorter flaps generally are far from the optimal region as shown later in Fig. 10. After the hydrodynamics properties are computed, the PTO and controls were optimized for each geometry (Section 3.1) according to the procedures in Sections 3.2 and 3.3, respectively. The maximum rotational amplitude constraint was set equal to 30° to allow for 60° of total pitch motion and the maximum PTO torque was left unconstrained so as not to restrict the optimal design. The results from the geometry optimization are illustrated with Fig. 10. The maximum power potential is obtained by assuming Eq. (4) for each frequency component of the wave excitation. With no rotational amplitude constraint enforced, this upper bound is an overestimation and may not be feasible in practice. The mechanical and electrical power, on the other hand, are obtained with maximum rotational amplitudes enforced. They are corresponding to the input and output of the two-port model as shown in Fig. 4. It is found the largest flap led to the largest potential power, while the widest flaps with a height of around 8 m led to the largest electrical power harvest. But, as discussed in Section 3.1, it is important to consider both the energy harvesting capabilities and the estimated cost of the system. The objective function (Eq. (20)) is defined as the electrical power output normalized by a cost factor defined with the surface area of the flaps. The parameters are selected as $k_1 = 6$, $k_2 = 4$ and $n = 1.6$, roughly corresponding to a 3:2 cost ratio between the first and second types of costs for the smallest flap and a 10:1 cost ratio for the largest flap. This objective function is used to identify a geometry with a height of 10 m and a width of 12 m as the optimal design. It is important to note that for the 8.33 s characteristic period wave spectrum considered for this study, the wavelength is around 100 m, which makes the 12 m optimal design more of a point absorber working in the surge mode [44]. In fact, all flaps with width shorter than 30 m exhibit point absorber characteristics, with their capture width ratio well above 100%.

It is also important to recognize the optimization setup may not account for all design factors. Often, the amplitude and PTO torque are of large importance to the robustness needed for an oscillating-surge WEC system and mooring. Although the surface area is considered as a cost proxy due to its major contribution to full-scale WEC cost [39], an extreme result for the maximum required torque or amplitude may result in an added expense or unrealistic design. In terms of WEC motion, most of the optimal designs have the same maximum position due to the amplitude constraint. On the other hand, the PTO torque requirements experience more variation, with some similarly effective designs requiring smaller PTO torques. Although the smaller PTO torques may have design benefits, none are extremely large, indicating that the current optimal design (w = 12 m, h = 10 m - Fig. 11) can be accepted because the material costs, which are related to surface area, are the main factor in the cost of full-scale WECs.

Table 1
Optimal PTO parameters.

PTO parameters	Optimal values
Gear ratio $\mathbf{N}$	500
Drivetrain inertia $\mathbf{I_d}$	20 kg m^2
Generator torque constant $\mathbf{K_t}$	12 N m/A
Drivetrain damping $\mathbf{B_d}$	2 N m s (constant)
Drivetrain stiffness $\mathbf{K_d}$	0 N m/rad (constant)
Winding resistance $\mathbf{R_w}$	0.038 Ω (constant)
Winding inductance $\mathbf{L_w}$	1.4 mH (constant)

For the optimal geometry selected, the optimized PTO components are detailed in Table 1. The time-series results for the optimized design can be found in Fig. 12.

The optimized system requires a maximum PTO Torque of 16,600 kN m (33.2 kN m to the generator) and a maximum amplitude equal to the specified amplitude constraint (30°), while producing an average electrical power output of 274 kW.

Since the simulated flap pierces the surface by 1 m, the effective height is equal to 1 m less than the specified height. Thus, the optimal flap has a width of 12 m and immersed height of 9 m, meaning a width to height ratio of 1.33. This result is in contrast to [9], which suggests a width to height ratio between 2 and 5 for irregular waves. The difference is believed to be mainly due to the costs that are factored into this study. It is clear from Fig. 10 that the power does in fact increase as the width increases, but the increased power of a design with a much larger width is outweighed by the increased surface area. The lack of consideration of cost in [9] leads to designs that may produce large amounts of power but are relatively expensive. By including PTO dynamics and a cost function in the optimization procedure, a greater understanding of a realistic optimal OSWEC design is achieved.

4.2. Control co-design advantages analysis

In this section, the importance of the application of co-design principles is assessed. First, maximization of electrical power and maximization of mechanical power are compared. Then, the co-design optimization procedure, which selects the optimal geometry based on electrical power maximization, is compared to a sequential design process where the optimal geometry is decided based on mechanical power maximization.

4.2.1. Electrical vs. Mechanical power maximization

Understanding the effect of electrical power maximization using a wave-to-wire (considers entire process from wave excitation forces to electrical power harvest) model is required to grasp the impact of applying co-design principles. For the optimized flap design determined in Section 4.1 (w = 12 m, h = 10 m) with its optimized PTO system, the pseudo-spectral method was used to optimize an unstructured controller first to maximize electrical power, then separately to maximize mechanical power (Table 2). Although the resulting position and velocity are similar, the mechanical power maximization leads to a larger torque and much higher electrical measurements (current and voltage). The maximum position and velocity similarities are most likely due to the amplitude constraint inherent to OSWEC devices. It is worth noting a looser constraint, such as with a point absorber WEC, would very likely lead to larger displacement and velocities as well as amplifying forces further. The larger torque, current, and voltages needed for mechanical power maximization would require both a higher-rated

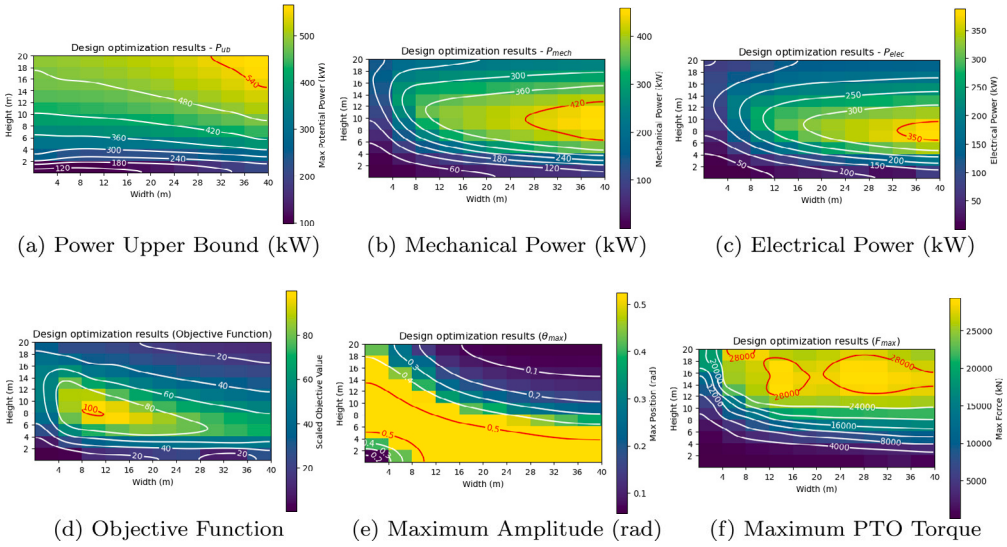

Fig. 10. Co-design optimization loop results.

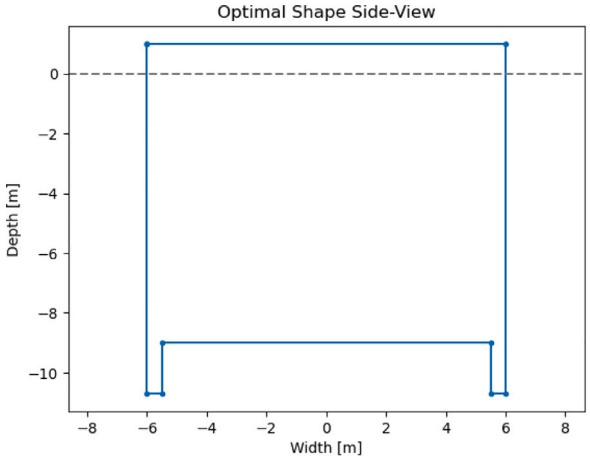

Fig. 11. Optimal geometry side-view.

mechanical and electrical system, increasing cost. Further, although the mechanical power maximization leads to a larger mechanical power (356 vs. 337 kW), the electrical power is significantly lower (187 vs. 274 kW) due to higher PTO losses. On the other hand, the electrical power maximization leads to effective control that factors in the power take-off system to increase the electrical power. The time-series plots for this comparison are shown in Fig. 13 and the results are summarized in Table 2.

In order to further understand the effect of electrical power maximization, two other cases were studied: one with looser amplitude constraints (60 degrees) and another with a non-optimal power take-off, the results for each of these cases are also summarized in Table 2. By allowing a larger range of motion, the case with looser amplitude constraints is likely similar to a heaving point absorber which is not limited by rotational motion constraints. The allowance of large pitch displacement leads to the controller attempting to enhance the motion, requiring large PTO torques and leading to a small electrical power when maximizing the mechanical power, both of which would be undesirable and expensive. The non-optimal PTO case is relatively similar. Although the amplitude constraint is still present, the system actually requires consuming larger amounts of electrical power to maximize mechanical power. In both cases, the electrical power maximization still leads to significant power, suggesting that the systems can still be viable, but only when properly evaluated with a consideration of usable electrical power. On the other hand, the mechanical power maximization leads to an inaccurate understanding of a design's realistic potential. Even though the looser amplitude constraints and non-optimal PTO may not be the most accurate or optimal representations, these results provide an opportunity to further understand the effects of the co-design optimization routine and the importance of electrical power maximization.

The above comparisons suggest the essential maximization of usable electrical power rather than mechanical power when performing any design optimization procedure. The intricacies of WEC design mean that the maximum mechanical power does not lead to the maximum electrical power and can require higher cost components. An optimization procedure with regard to electrical power ensures that the maximum usable output power is achieved, and the subsequent design is realizable and cost-efficient.

4.2.2. *Sequential design comparison*

In order to understand the benefits of the full co-design optimization procedure carried out within this paper, a comparison to the sequential design process can be made. For the sequential design process, an optimal geometry must be selected before optimizing the power take-off and controls. By considering the optimized mechanical power for each shape and normalizing the power by the cost factor, an optimal geometry can be selected as in Fig. 14 with a width of 8 m and a height of 16 m. Next, in accordance with the sequential design process, the power take-off was optimized together with a PI controller before finally optimizing the fine control using the pseudo-spectral method. The optimized power take-off parameters for this design are the same as the PTO of the co-designed optimal flap shape in Table 1. The reason is that the three optimized parameters all tend to the constrained limits for the targeted wave spectrum.

Ultimately, this sequential design process led to an electrical power output of 182 kW and an objective function value of 59.5 (Table 3). The optimal design as defined by the co-design process (Section 4.1) offers a 50.5% improvement in electrical power, but it is again important to consider the costs associated with the larger sizes of the geometry identified by the sequential design process. By normalizing the electrical power by the cost proxy, a significant 61.4% increase in the objective function is observed for the co-design optimization process over sequential optimization. Another factor to consider is the required

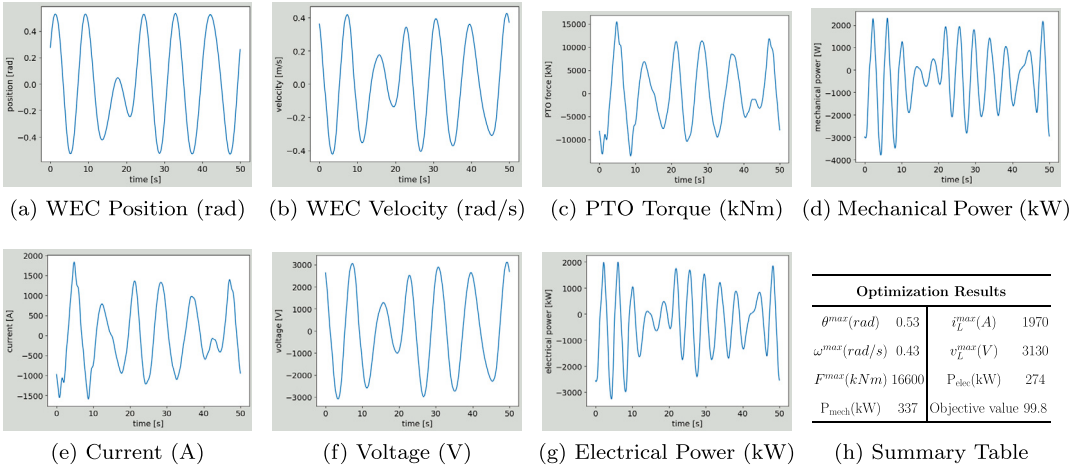

(a) WEC Position (rad) (b) WEC Velocity (rad/s) (c) PTO Torque (kNm) (d) Mechanical Power (kW)

(e) Current (A) (f) Voltage (V) (g) Electrical Power (kW)

Optimization Results			
$\theta^{max}(rad)$	0.53	$i_L^{max}(A)$	1970
$\omega^{max}(rad/s)$	0.43	$v_L^{max}(V)$	3130
$F^{max}(kNm)$	16600	P_{elec}(kW)	274
P_{mech}(kW)	337	Objective value	99.8

(h) Summary Table

Fig. 12. Time-series results for optimal OSWEC design.

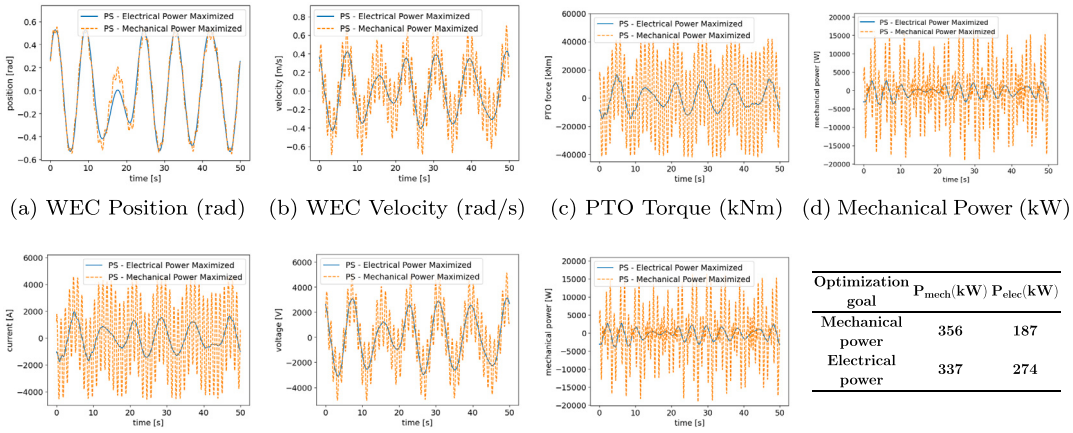

(a) WEC Position (rad) (b) WEC Velocity (rad/s) (c) PTO Torque (kNm) (d) Mechanical Power (kW)

(e) Current (A) (f) Voltage (V) (g) Electrical Power (kW)

Optimization goal	P_{mech}(kW)	P_{elec}(kW)
Mechanical power	356	187
Electrical power	337	274

(h) Summary Table

Fig. 13. Comparison of the maximization of mechanical power versus the maximization of electrical power for an optimized system with tight amplitude constraints.

Table 2
Results under different optimization setups.

Optimization goal	Constraints	PTO	θ^{max} (rad)	ω^{max} (rad/s)	F^{max} (kN m)	P_{mech} (kW)	i_L^{max} (A)	v_L^{max} (V)	P_{elec} (kW)
Mechanical power	30 degree maximum amplitude	Optimal PTO	0.54	0.59	31200	356	3490	3410	187
Electrical power	30 degree maximum amplitude	Optimal PTO	0.53	0.43	16 600	337	1970	3130	274
Mechanical power	60 degree maximum amplitude	Optimal PTO	1.06	0.96	41 400	430	4660	7050	95.2
Electrical power	60 degree maximum amplitude	Optimal PTO	0.9	0.59	19 300	369	2290	4320	285
Mechanical power	30 degree maximum amplitude	Non-optimal PTO	0.55	0.69	41 800	375	9970	2660	–881
Electrical power	30 degree maximum amplitude	Non-optimal PTO	0.53	0.4	13 100	297	3190	1560	202

Table 3
Comparison between results of sequential and co-design optimization routines.

	θ^{max} (rad)	ω^{max} (rad/s)	F^{max} (kN m)	P_{mech} (kW)	i_L^{max} (A)	v_L^{max} (V)	P_{elec} (kW)	ObjF
Sequential design	0.48	0.32	27 300	291	3540	2300	182	59.5
Co-design	0.53	0.43	16 600	337	1970	3130	274	99.8
Improvement (%)							**50.5**	**61.4**

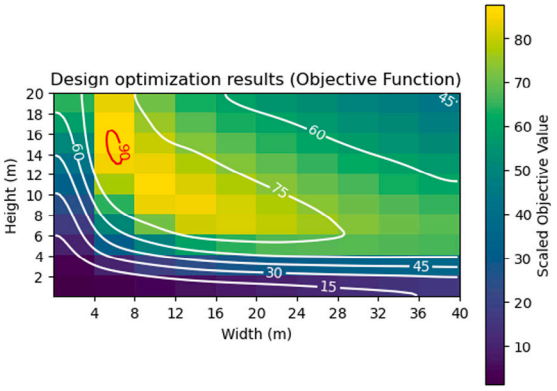

Fig. 14. Sequential design objective function results.

power take-off torque which, for the design from the sequential design process, is almost twice that of the co-design optimal design, meaning the PTO system would incur much higher costs. The key difference highlighted by this study is in the determination of optimal geometry. While a sequential design process determines optimal geometry based on the potential mechanical power, the co-design process here calculates the electrical power using optimal PTO and control to select an optimal geometry. Essentially, the consideration of the power take-off and control systems within the geometry optimization, as conducted with the co-design optimization procedure, has the potential to lead to very significant improvements in multiple facets and subsystems within WEC design.

4.3. Power take-off analysis for optimized flap

After determining an optimal design, it is crucial to ensure the design is both realistic and robust. In the optimization procedure carried out in this paper, the gear ratio, torque constant, and drivetrain inertia were assumed to be able to take on any value within the specified range. In reality, realization of these variables is not always feasible. For instance, the cheapest solution for a gearbox may be a commercial-off-the-shelf (COTS) option, which would likely have a few set gear ratio values to choose from. In order to assess the optimized PTO system, Fig. 15 displays a sensitivity analysis for the drivetrain including the gear ratio, drivetrain inertia, drivetrain friction, and drivetrain stiffness The sensitivity analysis informs the design team regarding which components may be able to be compromised on and which are paramount to maintaining a high electrical power.

In Fig. 15, it is clear that the drivetrain damping significantly affects the electrical power output and any increase will lead to a drastic decrease in power. The drivetrain damping (also known as mechanical friction) is always important to minimize, but the sensitivity analysis allows for an understanding of how impactful any adjustments will be. The results of a change in drivetrain damping suggested by the sensitivity analysis can be used in combination with component costs to drive effective decision making. On the other hand, the gear ratio and drivetrain inertia both have a much smaller effect on the power output and may even be worth compromising on to save costs. Lastly, the drivetrain stiffness has very negligible effects on the electrical power.

Next, a sensitivity analysis of the generator parameters was performed. This analysis may be particularly important due to the trade-offs that are often necessary in generator selection. For instance, increasing the torque constant often increases the winding resistance as well. Fig. 16 shows the sensitivity of the generator parameters. As expected, increasing the torque constant increases the electrical power, but an increase in winding resistance decreases the harvested electrical power. Thus, the effects of increasing torque constant can be effectively considered alongside the effects of increasing the winding resistance

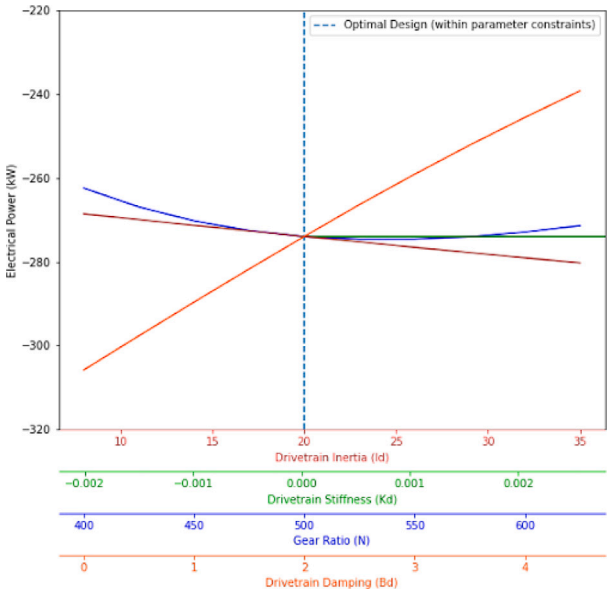

Fig. 15. Drivetrain sensitivity analysis.

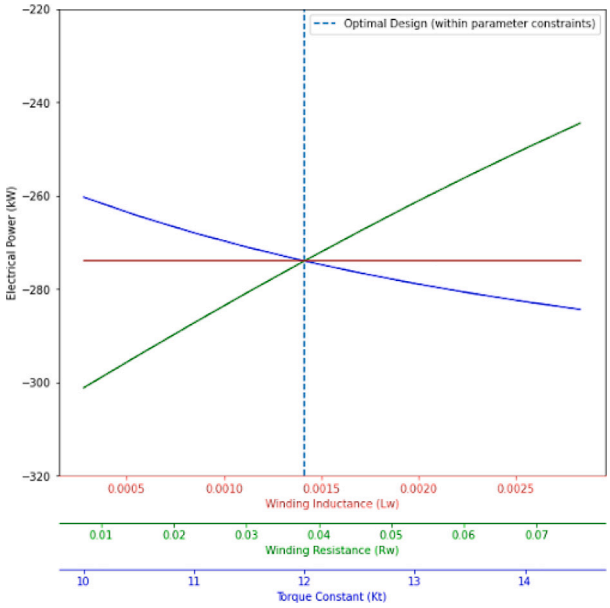

Fig. 16. Generator sensitivity analysis.

while also factoring in the costs. The winding inductance seems to have very little effect on the electrical power, so should not be prioritized when selecting a generator.

The last power take-off parameter to analyze is a torque limit. The torque limit corresponds to the rated torque of a selected generator. An increase in the rated torque generally correlates to an increase in the cost of the generator, but also allows for more energy to be harvested. Therefore, a sensitivity analysis of the PTO torque constraint can show how the selection of a PTO with a lower rated torque (less expensive) than desired will affect electrical power. Fig. 17 shows the sensitivity for the torque constraint. When the torque constraint is over about 20 kN m, the differences are relatively small with a torque limit of at least 25 kN m required for maximum power. On the other hand, tighter constraints lead to increasingly larger reductions in electrical power. These differences can be evaluated with cost to select a generator that is relatively inexpensive without sacrificing significant electrical power.

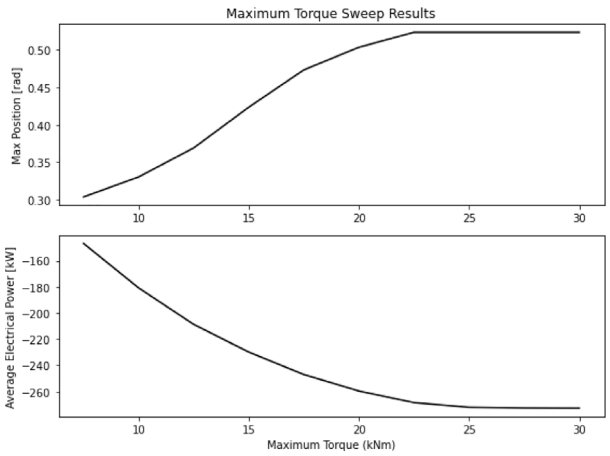

Fig. 17. Torque constraint sensitivity analysis.

4.4. Wave conditions analysis

The optimization results from Section 4.1 provide a valuable insight into the optimal design for an OSWEC in those specific wave conditions. On the other hand, the results offer little information on how the optimal design may be adapted to different wave conditions. In this section, an analysis of the effects of wave period and wave height on the optimal design is completed. In order to complete this analysis, a range of wave period and wave height values were utilized within the co-design optimization procedure. Although an irregular wave may be more representative of a realistic sea state, the regular wave provides a simpler method to assess wave period and height without unnecessary complications.

The results from the wave period analysis are displayed in Table 4 with the wave height kept constant at 2 m. As the wave period increases it is clear that the optimal width and height both increase, meaning a longer wave requires a larger OSWEC design for optimality. Further, the optimal width increases at a faster rate, meaning the optimal width to height ratio also increases with increasing period (0.67 to 2.57). The results from the wave height analysis are displayed in Table 5. Similarly to when increasing the wave period, larger wave heights lead to larger optimal OSWEC designs in terms of both width and height. It is clear that the optimal flap height is just slightly affected by wave height as it only increases from 8 m to 10 m throughout the entirety of wave heights modeled. Due to the larger increase in optimal width, the width to height ratio increases from a value of 1 to 2. Through examination of the trends in the optimization plots, it is found that, for each wave condition, the optimal width and height lies along the boundary of the range of geometries that maximize the amplitude (reach the amplitude constraint). This trend can be seen in Fig. 10 and is even more apparent in Fig. 18 which shows the objective function and maximum position values for the analysis performed with a period of 14 s. The most optimal (yellow) designs match up to the boundary of the design region reaching the amplitude constraint (yellow). This relationship suggests that the optimal geometry is one in which the amplitude of oscillation just reaches the amplitude constraint when maximizing electrical power, but does not need to be restricted by the constraint. In other words, an optimal geometry is one that is not significantly hindered by the constraints but naturally maximizes the amplitude to the constraint value in the respective wave conditions. Of course, this trend does not account for all factors as there is a large transition region where the amplitude constraint is met. The use of surface area as the cost proxy likely rewards the designs with fairly even widths and heights. On the other hand, the electrical power increases significantly enough under larger wave conditions (period and height) to outweigh the surface area increases for larger widths.

5. Conclusions

Within this co-design investigation and optimization for a bottom-hinged oscillating-surge wave energy converter, the geometry, power take-off, and control subsystems have been optimized in one optimization loop to ensure a fully optimal design. The geometric design is defined by varying values for flap width and height, the mechanical power take-off is represented by a two-port system with a drivetrain and generator, and the controller is modeled as an unstructured controller capable of applying an optimal power take-off torque at each timestep. Electrical power normalized by a cost proxy for the WEC is used as the optimization objective. As a comparison, a sequential design procedure where mechanical power is used in selecting the optimal geometry is made to understand the benefits of co-design optimization. Lastly, the PTO and control subsystems are examined more in-depth to prepare for detailed design.

Through the optimization study, an optimal design with a width of 12 m and a height of 10 m was determined. This design led to a relatively considerable increase in the electrical power and a very significant increase (61.4%) in the objective function when compared to the result of a sequential design optimization. The success of the co-design optimization procedure and the electrical power maximization in this study serves to reiterate the significance and importance of applying co-design principles to WEC design.

An analysis of the power take-off components suggests the importance of maintaining low mechanical drivetrain friction, balancing the torque constant and winding resistance of the generator, and selecting a generator with a torque limit of 20 kN m or above if possible. The knowledge of these trends will be advantageous during PTO component selection, where specific costs will also need to be factored into decision making. Optimizations under different wave conditions suggest an increase in overall OSWEC size with larger wave conditions (period and height) as well as an increase in the width to height ratio.

5.1. Discussions and future work

The findings of this study suggest a specific OSWEC design within the reasonable constraints, but the study itself has several limitations.

First, the most glaring limitation is the restriction to one type of wave energy converter. By focusing on an OSWEC in the form of a cuboid in this study, the range of potential solutions was drastically limited, effectively making the problem feasible within the desired timeframe. Conversely, this restriction leaves out many potential geometric solutions. Similarly, there are other power take-off types such as hydraulic PTOs which could be investigated as well. An application of this co-design optimization philosophy to other WEC and PTO types could lead to a broader comparison that may have greater implications to the convergence of the ocean wave energy harvesting industry as a whole.

Another limitation is the optimization procedure itself due to the independent optimizations of the PTO and controller. As discussed in Section 3.2, the optimization of the power take-off is performed separately from the controls. Unfortunately, this method restricts that portion of the co-design optimization to be the same as a sequential optimization. Therefore, the power take-off may not be truly optimal for the control implementation, especially considering the added non-linearities introduced by the amplitude constraint.

Overall, this co-design optimization procedure currently serves as the initial design phase used to narrow down on a design. The exact details of the oscillating-surge WEC and its subsystems still need to be designed. Although the geometry is already defined by the optimal width, height, and thickness, the exact mass and material properties will need to be analyzed and selected. As discussed in Section 4.3, the power take-off components will need to be selected to achieve close to the optimal parameters with a consideration of the cost of each component and the respective trade-offs in performance. After

Table 4
Effect of wave period on optimal width and height.

Regular wave period (s) (H = 2 m)	Optimal width (m)	Optimal height (m)	Electrical power (kW)	Objective function value
4	4	6	87.1	97
6	8	8	308	182
8	12	10	567	216
10	20	10	844	218
12	24	12	976	190
14	24	12	992	193
16	36	12	1066	147

Table 5
Effect of wave height on optimal width and height.

Regular wave height (m) (T = 8.33 s)	Optimal width (m)	Optimal height (m)	Electrical power (kW)	Objective function value
0.5	8	8	27.3	16
1	12	8	144	64
1.5	12	10	356	135
2	12	10	567	216
2.5	16	10	1057	324
3	16	10	1396	428
3.5	20	10	2156	559

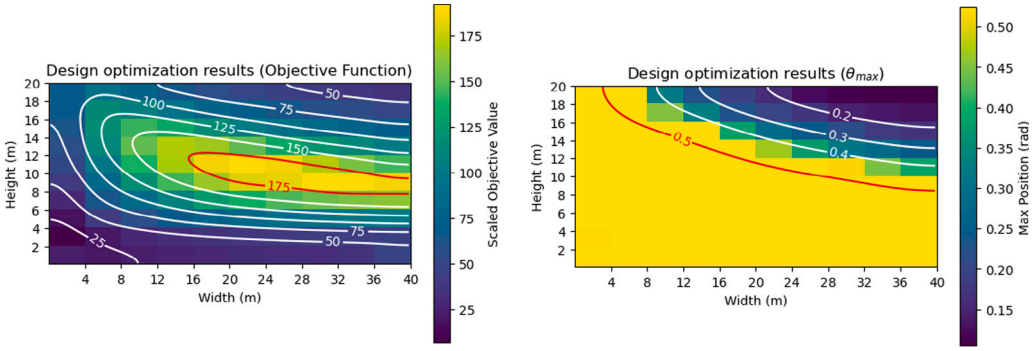

(a) Objective Function (kW/m^2) (b) Maximum Amplitude (rad)

Fig. 18. Results for T = 14 s.

selecting specific power take-off and controller components, rerunning the outer optimization loop with these components fixed would provide a valuable perspective on the sensitivity and precision of the co-design optimization. Ultimately, the findings of the current study provide an informative overview to support future detailed design decisions for the OSWEC device.

CRediT authorship contribution statement

Jeff Grasberger: Writing – original draft, Visualization, Investigation, Formal analysis, Data curation, Methodology, Software. **Lisheng Yang:** Writing – review & editing, Validation, Investigation, Data curation, Conceptualization, Methodology, Visualization. **Giorgio Bacelli:** Supervision, Software, Resources, Methodology, Funding acquisition, Formal analysis. **Lei Zuo:** Writing – review & editing, Supervision, Resources, Project administration, Funding acquisition.

Declaration of competing interest

The authors declare the following financial interests/personal relationships which may be considered as potential competing interests: Jeff Grasberger, Lisheng Yang reports financial support was provided by National Science Foundation.

Acknowledgments

The authors wish to thank the funding support from US National Science Foundation NSF via #2152694 and #1738689 as well as the US Department of Energy DOE seedling fund via #DE-NA0003525 for the research work presented in this paper. This paper describes objective technical results and analysis. Any subjective views or opinions that might be expressed in the paper do not necessarily represent the views of the US NSF, DOE, or the United States Government. The authors used the open source software WecOptTool [45] developed and maintained by Sandia National Laboratories in producing parts of the results presented in this paper.

References

[1] R.W. Bentley, Global oil & gas depletion: an overview, Energy Policy 30 (3) (2002) 189–205.
[2] K. Gunn, C. Stock-Williams, Quantifying the global wave power resource, Renew. Energy 44 (2012) 296–304.
[3] A. Clément, P. McCullen, A. Falcão, A. Fiorentino, F. Gardner, K. Hammarlund, G. Lemonis, T. Lewis, K. Nielsen, S. Petroncini, et al., Wave energy in Europe: current status and perspectives, Renew. Sustain. Energy Rev. 6 (5) (2002) 405–431.
[4] E. Al Shami, R. Zhang, X. Wang, Point absorber wave energy harvesters: A review of recent developments, Energies 12 (1) (2018) 47.
[5] N. Delmonte, D. Barater, F. Giuliani, P. Cova, G. Buticchi, Review of oscillating water column converters, IEEE Trans. Ind. Appl. 52 (2) (2015) 1698–1710.
[6] M. Folley, T. Whittaker, M. Osterried, The oscillating wave surge converter, in: The Fourteenth International Offshore and Polar Engineering Conference, OnePetro, 2004.

[7] T. Whittaker, M. Folley, Nearshore oscillating wave surge converters and the development of Oyster, Phil. Trans. R. Soc. A 370 (1959) (2012) 345–364.
[8] T.T. Loh, D. Greaves, T. Maeki, M. Vuorinen, D. Simmonds, A. Kyte, Numerical modelling of the WaveRoller device using OpenFOAM, in: Proceedings of the 3rd Asian Wave & Tidal Energy Conference, 2016.
[9] R. Gomes, M. Lopes, J. Henriques, L. Gato, A. Falcão, The dynamics and power extraction of bottom-hinged plate wave energy converters in regular and irregular waves, Ocean Eng. 96 (2015) 86–99.
[10] Y.-q. Zhang, S.-w. Sheng, Y.-g. You, Z.-x. Huang, W.-s. Wang, Study of hydrodynamic characteristics of a Sharp Eagle wave energy converter, China Ocean Eng. 31 (2017) 364–369.
[11] S. Sheng, K. Wang, H. Lin, Y. Zhang, Y. You, Z. Wang, A. Chen, J. Jiang, W. Wang, Y. Ye, Model research and open sea tests of 100 kW wave energy convertor Sharp Eagle Wanshan, Renew. Energy 113 (2017) 587–595.
[12] Y.-H. Yu, Y. Li, K. Hallett, C. Hotimsky, Design and analysis for a floating oscillating surge wave energy converter, in: International Conference on Offshore Mechanics and Arctic Engineering, Vol. 45547, American Society of Mechanical Engineers, 2014, V09BT09A048.
[13] N. Tom, M. Lawson, Y.-H. Yu, A. Wright, Development of a nearshore oscillating surge wave energy converter with variable geometry, Renew. Energy 96 (2016) 410–424.
[14] M. Kelly, N. Tom, Y.-H. Yu, A. Wright, M. Lawson, Annual performance of the second-generation variable-geometry oscillating surge wave energy converter, Renew. Energy 177 (2021) 242–258.
[15] M. Choiniere, J. Davis, N. Nguyen, N. Tom, M. Fowler, K. Thiagarajan, Hydrodynamics and load shedding behavior of a variable-geometry oscillating surge wave energy converter (OSWEC), Renew. Energy 194 (2022) 875–884.
[16] N. Nguyen, J. Davis, K. Thiagarajan, N. Tom, S. Husain, Investigation of theoretical solutions to a bottom-raised oscillating surge wave energy converter (OSWEC) through experimental and parametric studies, in: International Conference on Offshore Mechanics and Arctic Engineering, Vol. 86908, American Society of Mechanical Engineers, 2023, V008T09A082.
[17] Y.-H. Yu, D. Jenne, R. Thresher, A. Copping, S. Geerlofs, L. Hanna, Reference Model 5 (RM5): Oscillating Surge Wave Energy Converter, Tech. rep., National Renewable Energy Lab.(NREL), Golden, CO (United States), 2015.
[18] A. Trueworthy, B. DuPont, The wave energy converter design process: Methods applied in industry and shortcomings of current practices, J. Mar. Sci. Eng. 8 (11) (2020) 932.
[19] C. Beels, P. Troch, J.P. Kofoed, P. Frigaard, J.V. Kringelum, P.C. Kromann, M.H. Donovan, J. De Rouck, G. De Backer, A methodology for production and cost assessment of a farm of wave energy converters, Renew. Energy 36 (12) (2011) 3402–3416.
[20] V. Piscopo, G. Benassai, R. Della Morte, A. Scamardella, Towards a cost-based design of heaving point absorbers, Int. J. Mar. Energy 18 (2017) 15–29.
[21] V. Piscopo, G. Benassai, R. Della Morte, A. Scamardella, Cost-based design and selection of point absorber devices for the mediterranean sea, Energies 11 (4) (2018) 946.
[22] A. Rashid, M. Sidenmark, C. Eskilsson, M. Wallentin, IWEC–model validation and cost optimization of infinity WEC wave energy converter, in: 14th European Wave and Tidal Energy Conference 5-9th Sept 2021, Plymouth, UK, 2021, 2192–1.
[23] R. McCabe, O. Murphy, M. Haji, Multidisciplinary optimization to reduce cost and power variation of a wave energy converter, in: International Design Engineering Technical Conferences and Computers and Information in Engineering Conference, Vol. 86229, American Society of Mechanical Engineers, 2022, V03AT03A023.
[24] A. Garcia-Teruel, D. Forehand, Optimal wave energy converter geometry for different modes of motion, Adv. Renew. Energ. Offshore (2018) 299.
[25] A. Kurniawan, T. Moan, Optimal geometries for wave absorbers oscillating about a fixed axis, IEEE J. Ocean. Eng. 38 (1) (2012) 117–130.
[26] N.Y. Sergiienko, L.S.P. da Silva, B. Ding, B.S. Cazzolato, Importance of drivetrain optimisation to maximise electrical power from wave energy converters, IET Renew. Power Gener. 15 (14) (2021) 3232–3242.
[27] G. Bacelli, Optimal Control of Wave Energy Converters (Ph.D. thesis), National University of Ireland, Maynooth (Ireland), 2014.
[28] A.C. O'Sullivan, G. Lightbody, Co-design of a wave energy converter using constrained predictive control, Renew. Energy 102 (2017) 142–156.
[29] M. Garcia-Sanz, Control Co-Design: an engineering game changer, Adv. Control Appl.: Eng. Ind. Syst. 1 (1) (2019) e18.
[30] N. Faedo, J. Ringwood, A control design framework for wave energy devices, 2021.
[31] G. Bacelli, R.G. Coe, Comments on control of wave energy converters, IEEE Trans. Control Syst. Technol. 29 (1) (2020) 478–481.
[32] C.A.M. Ströfer, D.T. Gaebele, R.G. Coe, G. Bacelli, Control co-design of power take-off systems for wave energy converters using WecOptTool, IEEE Trans. Sustain. Energy (2023).
[33] A. Babarit, G. Delhommeau, Theoretical and numerical aspects of the open source BEM solver NEMOH, in: Proceedings of the 11th European Wave and Tidal Energy Conference, EWTEC2015, Nantes, France, 2015.
[34] M. Ancellin, F. Dias, Capytaine: a Python-based linear potential flow solver, J. Open Source Softw. 4 (36) (2019) 1341, http://dx.doi.org/10.21105/joss.01341.
[35] C. Geuzaine, J.-F. Remacle, Gmsh: A 3-D finite element mesh generator with built-in pre-and post-processing facilities, Internat. J. Numer. Methods Engrg. 79 (11) (2009) 1309–1331.
[36] D.J. Inman, R.C. Singh, Engineering Vibration, vol. 3, Prentice Hall, Englewood Cliffs, NJ, 1994.
[37] J. Falnes, M. Perlin, Ocean waves and oscillating systems: Linear interactions including wave-energy extraction, Appl. Mech. Rev. 56 (1) (2003) B3.
[38] R.G. Coe, G. Bacelli, D. Forbush, A practical approach to wave energy modeling and control, Renew. Sustain. Energy Rev. 142 (2021) 110791.
[39] A. Garcia-Teruel, D. Forehand, A review of geometry optimisation of wave energy converters, Renew. Sustain. Energy Rev. 139 (2021) 110593.
[40] P. Virtanen, R. Gommers, T.E. Oliphant, M. Haberland, T. Reddy, D. Cournapeau, E. Burovski, P. Peterson, W. Weckesser, J. Bright, et al., SciPy 1.0: fundamental algorithms for scientific computing in Python, Nature Methods 17 (3) (2020) 261–272.
[41] G. Bacelli, J.V. Ringwood, Numerical optimal control of wave energy converters, IEEE Trans. Sustain. Energy 6 (2) (2014) 294–302.
[42] T. Reveyrand, Multiport conversions between S, Z, Y, h, ABCD, and T parameters, in: 2018 International Workshop on Integrated Nonlinear Microwave and Millimetre-Wave Circuits, INMMIC, IEEE, 2018, pp. 1–3.
[43] K. Hasselmann, T.P. Barnett, E. Bouws, H. Carlson, D.E. Cartwright, K. Enke, J. Ewing, A. Gienapp, D. Hasselmann, P. Kruseman, et al., Measurements of wind-wave growth and swell decay during the Joint North Sea Wave Project (JONSWAP), Ergaenzungsheft Dtsch. Hydrogr. Z. Reihe A (1973).
[44] S. Jin, S. Zheng, D. Greaves, On the scalability of wave energy converters, Ocean Eng. 243 (2022) 110212.
[45] Sandia National Laboratories, WecOptTool, 2022, URL https://snl-waterpower.github.io/WecOptTool/.